Increasing precipitation due to climate change could partially offset the impact of warming air temperatures on glacier loss in the monsoon-influenced Himalaya until 2100 CE

Anya M. Schlich-Davies[1], Ann V. Rowan[2], Andrew N. Ross[1], Duncan J. Quincey[3], Vivi K. Pedersen[4]

[1]Priestley International Centre for Climate, School of Earth and Environment, University of Leeds, UK
[2]Department of Earth Science, University of Bergen and Bjerknes Centre for Climate Research, Bergen, Norway
[3]School of Geography, University of Leeds, UK
[4]Department of Geoscience, Aarhus University, Aarhus C, Denmark

Correspondence to: Ann V. Rowan (ann.rowan@uib.no)

Abstract. Glacier volume in the Himalaya is projected to shrink by 53–70% during this century due to climate change. However, the impact of changes in precipitation amount and distribution on future glacier change remains uncertain because mesoscale meteorology is not represented in current models that project glacier change. We explored the combined effects of past and future changes in air temperature and precipitation amount and distribution on the evolution of a benchmark glacier in the monsoon-influenced Nepal Himalaya—Khumbu Glacier in the Everest region of Nepal. Our climate-glacier modelling approach forced an ice-dynamical glacier evolution model with mass balance calculated using mesoscale meteorological variables derived from downscaling of Regional Climate Model outputs. Our simulations show that historical warming during the late Holocene will cause glacier volume loss of 10–23% during this century. Under moderate future warming (RCP4.5) from the present day, Khumbu Glacier could lose 70% volume by 2100 CE due to increasing air temperatures. Projected increases in precipitation in tandem with climate warming could offset half of this loss, reducing the volume lost by 2100 CE to 34%. Extreme future warming (RCP8.5) will not be compensated by changes in precipitation but will instead result in substantial ablation above 6,000 m, causing the highest glacier on Earth to vanish between 2160–2260 CE.

1. Introduction

Projecting glacier change in response to climate change is important for determining the impact of anthropogenic warming on regional water availability (Pritchard, 2019). However, such projections remain challenging because accumulation and ablation processes in mountain environments are driven by orographic feedbacks between high-relief topography and atmospheric circulation systems such as the South Asian Summer Monsoon (Bookhagen and Burbank, 2006). Glaciological processes such as the formation and evolution of supraglacial debris, which cover 4–7% of glacier surfaces globally and 30% of the glacier ablation areas in the Himalaya, further modify glacier response to climate change away from the trends predicted from regional mass balance calculations (Herreid and Pellicciotti, 2020; Kraaijenbrink et al., 2017; Rounce et al., 2023; Rowan et al., 2015). Projections of glacier evolution in the Himalaya therefore need to account for the feedbacks between debris transport, mass balance, and ice flow (Nicholson et al., 2021) that promote a longer dynamic response compared to climatically equivalent clean-ice glaciers (Rowan et al., 2015). High Mountain Asia is projected to lose $34 \pm 19\%$ of glacier volume by 2100 CE if warming is limited to 1.5°C to meet the ambitious Paris Agreement target (Kraaijenbrink et al., 2017). More realistic projections of glacier change give $53 \pm 23\%$ volume loss under the moderate warming scenario RCP4.5 and $69 \pm 20\%$ under the extreme warming scenario RCP8.5 (Kraaijenbrink et al., 2017; Marzeion et al., 2020; Rounce et al., 2023). Large uncertainties remain in projections of regional glacier change because of limitations in understanding of the interactions between the mass balance regimes of monsoon-influenced glaciers where accumulation and ablation both occur during the monsoon season and the dynamics of glaciers flowing through high-relief topography (Dehecq et al., 2019; Miles et al., 2018b; Salerno et al., 2023). In the monsoon-influenced Himalaya, changes in the extent and intensity of the Indian Summer Monsoon affected glacier expansion during the Last Glacial Maximum through changes in snowfall (Benn and Owen, 1998; Owen et al., 2009). Global Circulation Models (GCMs) project increasing Indian Summer Monsoon precipitation and variability with current global warming but do not accurately capture the orographic controls on mesoscale

57 meteorology (Katzenberger et al., 2021). Therefore the effects of future changes in the Indian Summer Monsoon
58 on glaciers in the monsoon-influenced Himalaya in terms of precipitation amount, timing, and phase (snow/rain)
59 remain poorly constrained (Immerzeel et al., 2012; Mölg et al., 2014; Ragettli et al., 2016; Shaw et al., 2022; Shea
60 et al., 2015).
61
62 Khumbu Glacier is a benchmark debris-covered glacier in the monsoon-influenced Himalaya and the highest
63 glacier on Earth, flowing from 7,981 m above sea level (a.s.l.) to 4,879 m a.s.l.; an elevation range that is
64 representative of the majority of glaciers in this region (Fig. 1). While satellite observations show that rates of
65 glacier mass loss across the Himalaya have accelerated over the last 40 years for both clean-ice glaciers and debris-
66 covered glaciers (Maurer et al., 2019), observations and models indicate that thick supraglacial debris has
67 historically reduce mass loss (King et al., 2020; Rounce et al., 2023; Rowan et al., 2021) but this dampening effect
68 is being overturned by the development of supraglacial ponds and ice cliffs within debris layers (Miles et al.,
69 2018a; Strickland et al., 2023). In common with many large Himalayan glaciers that are debris-covered, Khumbu
70 Glacier is in greater imbalance with climate than a climatically equivalent clean-ice glacier, and has maintained a
71 more extensive ice volumes than would be possible without supraglacial debris through the late Holocene (~2 ka).
72 However, recent rapid climate warming has caused extensive mass loss across the entire ablation area, with
73 maximum rates of surface lowering observed in the upper ablation area where the debris layer is thinnest (King
74 et al., 2020). As a result of greater mass loss occurring in the upper ablation area, the lower part of the ablation
75 area is dynamically detached from the active glacier such that ice does not flow from the accumulation area into
76 this section of the glacier (Rowan et al., 2021; Watson et al., 2017). This process of detachment and decay of the
77 former ablation area is extended in time for debris-covered glaciers by the insulation of the ice surface, such that
78 the terminus of the actively flowing glacier remains in contact with the detached ice tongue rather than receding
79 upvalley (Pellicciotti et al., 2015; Quincey et al., 2009; Rowan et al., 2021). The high proportion of debris-covered
80 glaciers in the monsoon-influenced Himalaya means that these processes will significantly affect regional glacier
81 evolution and yet few studies currently consider their impact (Rounce et al., 2023).
82
83 We used a novel climate-glacier modelling approach to simulate the evolution of Khumbu Glacier in the Everest
84 region of Nepal (Fig. 1) from the present day (2015 CE) until 2100 CE forced by three downscaled Regional
85 Climate Model (RCM) outputs under two Relative Concentration Pathways (RCPs; RCP4.5 and RCP8.5) (Collins
86 et al., 2013) and continued these simulations to 2300 CE using the best available projections of longer-term
87 climate change. The downscaled RCM outputs were used to calculate mass balance time slices using a surface
88 energy balance model, which then forced a 3-D glacier evolution model. We made six simulations from three
89 RCMs and two RCPs to explore the impacts of possible variability in future precipitation amount and distribution
90 in tandem with climate warming on glacier volume and dynamics. The experimental design represents an advance
91 compared with previous climate-glacier modelling efforts through including mesoscale meteorological
92 phenomena, processes that redistribute the surface mass balance including snow avalanching and sublimation,
93 and the feedbacks between supraglacial debris transport, mass balance, and ice flow. The climate-glacier model
94 experimental design used here aims to calculate mesoscale meteorology at an appropriate scale to represent the
95 mass balance of a high-elevation glacier in the monsoon-influenced Himalaya combined with a sophisticated
96 glacier evolution model to represent the processes occurring at the surface that significantly affect glacier mass
97 balance.
98
99 **2. Models and data**
100 **2.1 RCM downscaling using meteorological observations**
101 RCMs were assessed on their fidelity to present-day climate, also known as hindcasting (Biemans et al., 2013),
102 with emphasis on temperature seasonality and seasonal precipitation dynamics given the importance of these
103 variables for glacier mass balance. RCMs from the Coordinated Regional Downscaling Experiment (CORDEX)
104 South Asia domain dynamically downscaled from CMIP5 GCMs by the Indian Institute of Tropical Meteorology
105 to a 50 km spatial resolution (Lutz et al., 2016) were downloaded for the grid box nearest to Khumbu Glacier
106 (27.9065056°N, 86.4352951°E) at about 2,100 m a.s.l.. Three of the six available CORDEX South Asia RCMs
107 (NOAA, CCCma, IPSL) were selected to represent three discrete precipitation scenarios (Table 1); either wet,
108 moderate, or dry climate in 2080–2100 CE. The three RCMs span the range of possible future precipitation
109 scenarios and were downscaled using quantile mapping evaluated against observations from high-elevation
110 automatic weather stations (AWS). Observations from AWS (Fig. 1c) collected between January 2006 and
111 November 2019 were used to aid RCM downscaling with gaps filled with interpolated data from neighbouring
112 stations where possible (Fig. 2). Quantile mapping also known as "distribution mapping", was used to statistically
113 downscale the daily climate data using 14 years of observations from three AWS. Parametric quantile mapping
114 (Piani et al., 2010) was used whereby a statistical relationship between the raw climate model outputs and
115 observations is formed by substituting the RCM results with observations at a cumulative density function of the
116 prescribed distribution (e.g. a gaussian distribution for temperature; Luo et al., 2018; a gamma distribution for

precipitation; Piani et al., 2010). This correction was then applied to the raw RCM outputs to produce a third downscaled dataset to better match observations (Maraun, et al., 2016). The quantile mapping approach is effective for the challenge of downscaling of precipitation and reduces errors in the standard deviation, the coefficient of variation, and the skewness of distributed values relative to other methods (Lafon et al., 2012; Reiter et al., 2018). AWS data were used to disaggregate daily downscaled present-day and end-of-century climate model outputs to the hourly resolution required for the energy balance modelling using seasonal means to reproduce the 'nocturnal peak' seen during the monsoon. The MELODIST Python tool was used to disaggregate all other meteorological variables (Förster et al., 2016).

14 years of meteorological observations were derived from the two Pyramid AWS at 5,050 m a.s.l and at 5,035 m a.s.l and the West Changri Nup Glacier AWS at 5,363 m a.s.l.. Missing data were replaced through interpolation with an alternative AWS in this group. Precipitation was measured at 15-minute intervals using a Geonor T-200BM sensor mounted 1.8 m above the surface. Evaporation from the bucket is supposedly blocked by a layer of oil but some does occur as evidenced by precipitation values below 0 mm. Noise from wind and evaporation were corrected for by compensating any negative change over the 15-minute time step with the neighbouring positive value such that accumulated precipitation was unchanged. Periods with prolonged evaporation were set to zero. Undercatch of snowfall by rainfall gauges was corrected through precipitation phase partitioning using wind speed observations (Wagnon et al., 2009). For interpolation of air temperature, hourly lapse rates were used that averaged 0.00554 °C m^{-1} to adjust to the height of the reference point at 5,050 m a.s.l.. Where possible, precipitation data were taken from the Pyramid AWS at 5,035 m a.s.l. because this precipitation gauge provides a longer period of continuous observations than the other gauges and avoids errors due to low precipitation amounts measured by tipping bucket gauges, which are known to systematically underestimate snowfall, particularly during high winds (Sherpa et al., 2017).

2.2 RCM downscaling for representation of future climate
There are only two future climate scenarios (RCP4.5 and RCP8.5) for CORDEX South Asia. RCP4.5 and RCP8.5 represent moderate or extreme warming by 2100 CE relative to the present day and are frequently used in climate impact studies, enabling comparison of our results with other glacier model projections. The RCPs were analysed for each of the three CORDEX RCMs. The same statistical downscaling approach and disaggregation used for the present day RCMs was applied to the raw CORDEX RCM daily outputs for the future time slices under RCP4.5 and RCP8.5. Downscaled future climates were compared with those found in other studies using CORDEX results and we found similar annual and seasonal temperature trends for the region strongly linked to the choice of RCP, and positive precipitation trends with poor agreement between RCMs (Kaini et al., 2019; Sanjay et al., 2017). The relationship between precipitation and RCP was less clear than that for air temperature because the monsoon-influenced Himalaya shows particularly poor RCM consensus and high levels of uncertainty in future precipitation trends with warming relative to other regions in High Mountain Asia (Sanjay et al., 2017). Given the absence of regional climate projections beyond 2100 CE, global temperature change projections were applied to the end-of-century mass balances for RCP4.5 and RCP8.5 which gave an increases in temperature under RCP4.5 of 0.5 °C by 2200 CE and 0.7 °C by 2300 CE, and under RCP8.5 of 2.8 °C by 2200 CE and 4.1 °C by 2300 CE (Collins et al., 2013). No precipitation change was applied to the post-2100 CE climates due to the absence of projections for precipitation in the CORDEX RCMs.

2.3 Surface energy and mass balance calculation using COSIPY
The Coupled Snowpack and Ice-surface Energy and Mass Balance model in Python (COSIPY) was used to calculate surface energy balance (Sauter et al., 2020). COSIPY is developed and modularised in Python and integrates a surface energy balance model with a multi-layer snow and ice model and thereby resolves all energy fluxes at the ice surface that contribute to surface melt. COSIPY has previously been applied to glaciers in High Mountain Asia and includes a calculation of sublimation, which is an important ablation process for high-elevation glaciers (Bonekamp et al., 2021; Brun et al., 2023; Huintjes et al., 2015). The COSIPY model domain was taken from the 30-m digital elevation model (DEM) acquired from the Shuttle Radar Topography Mission (Farr et al., 2007) that was resampled to 100-m grid spacing. We used the topographic rather than subglacial surface to calculate annual clean-ice glacier surface mass balance to enable integration with the glacier model by making the domain for the mass balance calculations larger than the glacier area. CORDEX daily climate variables (temperature, precipitation, the radiation components, wind speed, relative humidity and atmospheric pressure) were used to force COSIPY. Snowfall measurements can be used as an input to COSIPY, however, given the paucity of observations and high uncertainties associated with the AWS observations, climate reanalysis and modelled products for this region, precipitation was partitioned into rainfall and snowfall using the snow transfer scheme within COSIPY (Sauter et al., 2020). COSIPY was forced using hourly meteorology with nine variables to calculate the energy balance and mass balance components at an hourly time step from the sum of accumulation by solid precipitation, deposition, and refreezing of melt water percolation, and ablation by melt and sublimation.

The impact of supraglacial debris on ablation rates and avalanching on accumulation rates was handled subsequently in the glacier evolution model.

2.4 Glacier evolution modelling using iSOSIA

The integrated second-order shallow ice approximation model (iSOSIA) is a 3-D higher-order ice-dynamical glacier evolution model that solves for the flow of ice including longitudinal and transverse stress gradients that are imposed on ice flow through high-relief topography (Egholm et al., 2011). While previous versions of this model used depth-integrated ice flow, the version used to simulate Khumbu Glacier in this and earlier studies is fully 3-D as the ice thickness is divided into 20 vertical layers to allow the calculation of englacial ice flow and debris transport (Rowan et al., 2015). iSOSIA has a variable time step that can adjust to allow greater computational efficiency to a maximum of 0.1 years. This glacier model simulates the evolution of debris-covered glaciers by incorporating the feedbacks between debris transport, mass balance and ice flow (Rowan et al., 2015). iSOSIA includes two processes that are important for many Himalayan glaciers—the redistribution of snow by avalanching that is estimated to provide 75% of glacier accumulation, and the formation of supraglacial debris layers that insulate the ice surface and significantly modify ablation (Fig. 1d) (Anderson and Anderson, 2016; Rowan et al., 2015).

The distributed mass balances calculated using COSIPY forced by downscaled RCM outputs were used as inputs to iSOSIA. Surface processes within the glacier model then modified the distribution of accumulation and ablation. Simulated accumulation was the result of the total snowfall in each cell and avalanching of snow imposed for the accumulated snowpack from hillslopes using a non-linear hillslope flux model by removing snow and ice from hillslopes greater than 28° and redistributing this mass across less steep surfaces using a non-linear hillslope flux model (Roering et al., 1999). The avalanching routine was previously applied to Khumbu Glacier and found to be sufficient to prevent snow and ice accumulation on slopes that are observed to be free of glacier ice such as the southwest face of Sagarmatha/Mt. Everest whilst allowing accumulation on steep sections of the glacier (Rowan et al., 2015). The critical slope of 28° was selected because this threshold is low enough to prevent ice accumulation on slopes that are clearly ice-free today, but high enough to produce accumulation rates at the glacier surface that are in line with the limited available observations for Himalayan glaciers (Benn and Lehmkuhl, 2000). Rock avalanching is responsible for much of the debris accumulation on the glacier surface, but there is little information about the magnitude and frequency of these events, and so debris delivery to the glacier accumulation area was assumed to be spatially and temporally uniform at a rate of 1 mm a^{-1} (Rowan et al., 2021). Debris was delivered to the glacier surface from headwall erosion using a similar non-linear hillslope flux model to the avalanching routine. The reduction in ablation beneath supraglacial debris from clean-ice values was represented as a reciprocal function that scales clean-ice ablation (b_{clean}) to give sub-debris melt (b_{debris}) as a function of debris thickness (h):

$$b_{debris} = b_{clean} \times \frac{h_0}{h + h_0} \qquad \text{Eq. (1)}$$

where h_0 is a constant representing the characteristic debris thickness at which the reduction in ablation due to insulation by supraglacial debris is 50% of the value for an equivalent clean-ice surface (Anderson and Anderson, 2016; Rowan et al., 2021). The observed heterogeneity of ablation on the surface of Khumbu Glacier requires a parameterisation of sub-debris melt that represents the effects of differential ablation, which is represented in Equation (1) by the value chosen for h_0 (Rowan et al., 2021). The value for h_0 of 0.8 m represents a positively skewed supraglacial debris thickness distribution that includes ablation 'hotspots' such as supraglacial ponds and ice cliffs and is representative of the current state of Khumbu Glacier (Bartlett et al., 2021; Rowan et al., 2021; Strickland et al., 2023).

3. Climate-glacier model experimental design

We made an ensemble experiment forced by three downscaled RCMs under two future climate scenarios (RCP4.5 and RCP8.5) using time slices representing the present day (2015–2020 CE) and the end of the 21st Century (2095–2100 CE). Climate time slices representing five-year periods were chosen to reduce the computational expense of the climate-glacier modelling (~24 hours per simulation) and the preceding decade was used for comparison with the climate time slices. The three RCMs represent a range of possible future climates; the NOAA RCM is characterised by the highest annual precipitation, the IPSL RCM is characterised by the lowest annual precipitation, and the CCCma RCM is characterised by an intermediate value. The results from the downscaled RCMs were used as inputs to the surface energy balance model and then the six mass balance calculations (present day and future for each RCM) were used to force the glacier model.

The glacier model parameterisation and experimental design followed our previous work (Rowan et al., 2021). Estimated ice thickness (Farinotti et al., 2019) was subtracted from the 30-m DEM to yield a subglacial

topography for the model domain. The ice-free model domain incorporated the full hydrological catchment including the steep hillslopes of the Western Cwm that provide snow by avalanching to the glacier surface. The total amount of snow accumulation across that catchment was calibrated such that the snow delivered to the glacier surface was equivalent to the estimated rate of glacier accumulation of about 2 m water equivalent (w.e.) per year (Benn and Lehmkuhl, 2000). Khumbu Glacier is surrounded by ice-marginal moraines denoting the late Holocene (1.3 ± 0.1 ka) extent and ice thickness (Hornsey et al., 2022), which are used to constrain the historical spin-up simulation. The late Holocene glacier was reconstructed using a 5000-year equilibrium simulation starting from an ice-free domain. The late Holocene glacier volume was used as the starting point for a transient simulation through the 'Little Ice Age' maximum forced by a step change in mean annual air temperature of 1.5°C. The simulations continued to the present day and 2100 CE forced by the distributed mass balances calculated using COSIPY. Observations and modelling of the dynamics and structure of Khumbu Glacier show that the lower 5 km (25% of the total length, 20% of total ice volume) is stagnant and has dynamically detached from the active glacier in the last century (Miles et al., 2021; Quincey et al., 2009; Rowan et al., 2021). Basal ice at the glacier surface indicates that the active terminus overrides the stagnant glacier tongue (Miles et al., 2021) and surface displacement measurements show no longitudinal ice flow through the detached debris-covered tongue, which is instead collapsing laterally at a rate of 3 m a^{-1} (Watson et al., 2017). We therefore simulated only the active section of the glacier and assigned the stagnant mass of the detached debris-covered tongue to the model domain as a static topographic feature.

The simulated present-day glacier was evaluated against a range of observations to identify the simulation forced using the NOAA RCM as the most representative starting point for future simulations. Mean annual air temperatures (MAAT) in the Khumbu Valley increased by 1.4 ± 0.4°C under RCP4.5 and 3.8 ± 0.2°C under RCP8.5 by 2100 CE relative to the present day (Sanjay et al., 2017). Greater warming occurred in winter than in summer under both RCPs (Sanjay et al., 2017) and warming air temperatures resulted in an increase in annual precipitation amount of ~15%, with a greater increase in winter precipitation than summer precipitation. As there are no regional temperature projections beyond 2100 CE we used global values to continue the simulations into the next century: between 2100 CE and 2200 CE a step change in warming for each of the 3 RCMs of 0.5°C for RCP4.5 and 2.8°C for RCP8.5 relative to 2100 CE was applied to simulate mass balance for 2200 CE consistent with our time slice approach for the 21st Century simulations. Between 2200 CE and 2300 CE, warming of 0.7°C for RCP4.5 and 4.1°C for RCP 8.5 relative to 2100 CE was applied to simulate mass balance for 2300 CE. There are also no global projections of precipitation beyond 2100 CE and rather than introduce potentially significant uncertainties into our results by estimating these values, no change in precipitation was applied beyond 2100 CE.

3. Results
3.1 Evaluation of the climate-glacier model results
The downscaled climate variables from the three RCMs for the present-day time slice were evaluated using 14 years of observations from AWS to assess the representation of means, seasonality, diurnal cycles, day-to-day variability, and interannual variability. Across the three present-day simulations, the mass balance calculated using the NOAA RCM was more positive than the ISPL and CCCma results and most similar to the mass balance calculated from meteorological observations.

The three downscaled RCMs show good agreement in their mean annual air temperatures (–2.15 ± 0.05°C) and in comparison with observed air temperatures from the Pyramid AWS. The representation of the monsoon was greatly improved by the RCM downscaling: Temperature seasonality was well resolved following quantile mapping and the monthly mean and minimum air temperatures were similar to observations (Fig. S1). In the downscaled RCMs, the monsoon stabilises air temperatures and reduces the range between minimum and maximum temperatures, which is in better agreement with AWS observations but does not occur if the raw RCMs are used. Downscaled maximum air temperatures were similar in distribution to observations but were slightly higher than observed values during the post-monsoon and winter for all RCMs, and the maximum air temperature from the NOAA RCM was slightly higher than observations in the pre-monsoon and monsoon periods (Fig. S2). Gamma distribution quantile mapping substantially improved the absolute precipitation values, with the result that the overestimation of winter precipitation and relative underestimation of monsoon precipitation amounts in the raw RCMs was reduced and the downscaled results showed a clearer monsoon signal (Fig. S3). When compared with AWS observations, RCM downscaling slightly over-corrected the seasonal precipitation pattern, with a slight underestimation of winter precipitation for the most extreme winter events.

The simulated glacier extents and dynamics were compared with observations of the present day state and recent (<50 years) change (Fig. 4). The distributed mass balance following integration with iSOSIA to include the effects of melt reduction beneath supraglacial debris was more similar to observations than the clean-ice mass balance forcing taken from COSIPY. The glacier extent was underestimated if supraglacial debris and avalanching of snow

were not simulated (Fig. 5). The representation of supraglacial debris transport in iSOSIA reproduces the observed reversed mass balance gradient giving the highest ablation rates just below the equilibrium line (Benn and Lehmkuhl, 2000). Simulated glacier area was 7.8 km^2 and similar to that from structural mapping approximately 40 years before present day in 1979 CE (Nakawo, 1986). Radio-echo sounding in 1999 CE obtained ice thickness estimates close to the active terminus of ~160 m (Gades et al., 2000) and simulated ice thickness at the terminus was 130 m. The simulated active terminus thickness was approximately 175 m in 1999 CE, which agrees well with observations of the glacier thinning here by up to 55 m between 1984 and 2018 (King et al., 2020). Simulated surface elevation change in the lower ablation area was –30 m over 20 years to the present day and similar to values derived from satellite observations for 1984–2015 CE (King et al., 2020).

Simulated glacier velocities (Fig. 6) reach a maximum of 220 m a^{-1} and agree closely with remote sensing observations (Altena and Kääb, 2020). The simulated present-day velocities that are a better fit to remote sensing observations than previous simulations using an elevation-dependent mass balance forcing (Rowan et al., 2015, 2021) where the maximum simulated velocities were 118 m a^{-1}. Altena and Kääb (2020) estimated velocities of just over 1 m d^{-1} through the Khumbu icefall using satellite image matching compared with mountaineers' navigation devices from May 2018. Feature-tracking estimates of the upper ablation area of Khumbu Glacier indicate velocities of up to 20 m a^{-1} (Quincey et al., 2009; Dehecq et al. 2019). The debris-covered tongue has dynamically detached from the active part of Khumbu Glacier (i.e. the upper ablation area and accumulation area). This implies that the active glacier and the stagnant debris-covered tongue evolve as two separate systems, with the debris-covered tongue in an advanced state of decay while ice flow continues through the active glacier.

3.2 Climate change and glacier evolution from the present day until 2100 CE

Downscaled RCMs used to calculate distributed mass balances for the present day and 2100 CE for each of the three RCMs under both RCPs, with the NOAA RCM experiment considered most representative of the present state of Khumbu Glacier and future glacier change. Projected glacier volume changes show differences between RCM experiments equivalent to 22% under RCP4.5 and 9% under RCP8.5 by 2100 CE resulting from differences in projected air temperature change and precipitation change and variability. The mean glacier volume loss by 2100 CE across the RCM ensemble is 0.399 × 10^6 m^3 (46%) under RCP4.5 and 0.506 × 10^6 m^3 (57%) under RCP8.5. The change in MAAT under RCP4.5 for the downscaled NOAA RCM was 1.4°C warmer than the present day (–0.75°C in 2095–2100 CE compared with –2.15°C in 2015–2020 CE). Annual precipitation increased by 14.8% from 581.4 mm in the present day to 664.8 mm a^{-1} in 2100 CE under RCP4.5, of which summer (JJAS) precipitation increased by 5.4% and winter (DJF) precipitation increased by 14.1%. The change in MAAT under RCP8.5 for the downscaled NOAA RCM was 3.8°C higher than present day (1.65°C in 2095–2100 CE). Annual precipitation increased by 14.9% in 2100 CE under RCP8.5, of which summer precipitation increased by 9.8% and winter precipitation increased by 19.4%. In the NOAA RCP4.5 experiment, MAAT warmed by 1.4°C by 2100 CE compared to warming of 1.6°C for the IPSL experiment and 2.2°C for the CCCma experiment. The CCCma RCP4.5 experiment projected loss of 57% by 2100 CE owing to a smaller projected increase in precipitation than the NOAA experiment. For the NOAA RCP8.5 experiment, MAAT warmed by 3.8°C by 2100 CE, compared to 3.9°C for the IPSL experiment and 4.1°C for the CCCma experiment, and the 15% projected increase in annual precipitation was not sufficient to offset glacier loss.

In the NOAA RCP4.5 experiment, glacier volume decreased by 36% between the present day and 2100 CE (Fig. 7). While significant, the end-of-century glacier loss was partially offset by the concurrent increase in precipitation amount. In comparison, an equivalent simulation forced only by warming and without any change in precipitation resulted in a more linear trajectory of glacier change and 70% loss of glacier volume by 2100 CE (Fig. 8), demonstrating that 34% of potential glacier loss resulting from warming air temperatures could be compensated by the changes in precipitation that will occur as a result of warming air temperatures. The resulting spatially averaged cumulative mass balance was –0.14 m w.e. a^{-1} in 2100 CE, which is slightly more positive than the present-day value of –0.21 m w.e. a^{-1}. Under RCP8.5, all experiments give similar results for mass balance by 2100 CE with only a 10% difference in glacier volume between RCMs (Fig. 7). The CCCma experiment has only a 1% difference in volume loss between RCP4.5 and RCP8.5 by 2100 CE despite a 1.9°C difference in MAAT. This is a surprising result given the significant temperature difference but it can be attributed to the greater number of high-magnitude precipitation events that occur under RCP8.5 in combination with the small difference in winter temperatures between the two RCPs. Indeed, in the CCCma experiment under RCP4.5, maximum winter temperature was 1.7°C higher than for the other RCMs, resulting in ablation and rainfall during the winter.

Khumbu Glacier is responding to historical climate change and would continue to shrink even if warming ceased today. Indeed, if we allow the spin-up experiment to reach equilibrium with the present-day NOAA RCM mass balance, the glacier terminus will recede by 2.1 km and the maximum ice thickness will decrease from 246 m to 206 m by 2100 CE without any additional warming (Fig.7a). In this simulation, a supraglacial debris layer up to

357 1.3 m thick extended 1 km up-glacier from the terminus and partially dampened the committed loss by sustaining
358 13% more ice volume than would be the possible for a clean-ice glacier surface under the same mass balance
359 conditions. Therefore the committed glacier volume loss due to historical warming and in the absence of any
360 further climate forcing is 10–23% of the present-day glacier volume (Fig. 7b). Therefore, keeping future warming
361 within the limit of RCP4.5 will limit further shrinking of Khumbu Glacier to only 26% beyond that already
362 committed to by historical climate change.

3.3 Climate change and glacier evolution from 2100 CE until 2300 CE
365 Projections of climate change beyond 2100 CE are more uncertain than those for this century, but do give rise to
366 a possible prognosis for Khumbu Glacier. In the RCP4.5 there was little change in glacier volume between 2200
367 CE and 2300 CE compared to 2100 CE regardless of the RCM forcing used (Fig. 7b). In the NOAA RCP4.5
368 experiment, the Khumbu Icefall is maintained through to 2300 CE such that ice continues to flow from the Western
369 Cwm to below 6,000 m and the glacier remains in contact with the dynamically detached tongue. Therefore under
370 RCP4.5 Khumbu Glacier could reach a new dynamic equilibrium that maintains a sufficient ice thickness to
371 protect against catastrophic mass loss for at least two centuries. However, substantial glacier loss occurred after
372 2100 CE in all the RCP8.5 experiments and as a result, Khumbu Glacier completely decayed before 2300 CE.
373 Physical detachment of the debris-covered tongue from the active glacier occurred around 2070 CE in the CCCma
374 and IPSL experiments and around 2140 CE in the NOAA experiment (Fig. 6). We define the glacier to be stagnant
375 at flow at rates less than 10 m a^{-1}, which is a conservative estimate of the uncertainty associated with observations
376 of glacier velocities (Dehecq et al., 2019). Accordingly, we consider Khumbu Glacier to no longer be a viable
377 glacier system at the point where there is no ice flow above this value in the entire glacier since there is minimal
378 throughput of mass through the ice volume. In the NOAA RCP8.5 experiment, the glacier area was 1.2 km^2 and
379 the mean velocity reduced to 10 m a^{-1} by 2260 CE, such that the glacier was no longer viable as an active system.
380 Glacier breakdown occurred earlier for the CCCma and IPSL RCMs because loss of ice volume due to warming
381 was not compensated to the same magnitude by an increase in precipitation as that projected under RCP8.5 using
382 the NOAA RCM.

4. Discussion
4.1 Uncertainties associated with the climate-glacier modelling approach
386 The climate-mass balance forcing ensemble was limited in size due to the small number of different RCMs
387 available for the CORDEX South Asia region, and we considered all the relevant available forcings. A single
388 RCM was not considered sufficient to represent both present-day climate and potential future climatic extremes.
389 The use of three RCMs allows the implications of uncertainties in understanding of local climate for glacier
390 evolution to be simulated. The differences in simulated glacier change and response time that result from the RCM
391 forcings are at times greater than those arising from the choice of RCP due to varied projections of precipitation.
392 The CORDEX CMIP5 and CMIP6 projects only produced dynamically downscaled RCMs for RCP4.5 and
393 RCP8.5 and so the implications of other RCPs for glacier evolution cannot yet be assessed in our study. A multi-
394 model mean approach, which is widely used elsewhere, was not considered sufficient to represent present-day
395 and future climate conditions in the Khumbu Valley as this approach gives equal weighting to models with poor
396 and good performance in reproducing climate (Pierce et al., 2009). The representation of the distribution and rates
397 of accumulation were improved following integration of the RCM-forced mass balances with iSOSIA because the
398 redistribution of snowfall by avalanching from hillslopes onto the glacier improves agreement between simulated
399 accumulation rates and expected values for Himalayan glaciers (Benn and Lehmkuhl, 2000). Future work to
400 resolve the impact of low frequency–high magnitude avalanche events on accumulation rates would help to refine
401 this calculation but the contribution of avalanches to glacier accumulation over decadal time scales remains
402 challenging to measure.

404 Five-year downscaled RCM time slices were chosen to reduce computational expense associated with COSIPY
405 and the integration with iSOSIA. To ensure the selected five years were representative of the climate for that
406 period, the preceding decade was also used for comparison with the time slice climate results, although the
407 quantile mapping downscaling method using 14 years of reference AWS data should limit the influence of any
408 natural variability (i.e., by ensuring that the period is not reflecting an extreme phase of natural climate
409 oscillation). This comparison was particularly important for the future time slices where large uncertainties arise
410 between RCMs and there are no observations for evaluation of downscaled climate or mass balance. Information
411 on signal and variability between the present day (2015–2020 CE) and the future (2095–2100 CE) is not included
412 in the modelling approach. An experiment was conducted using mid-century mass balance forcings to investigate
413 the effect on glacier-climate imbalance. However this experiment produced identical results to the experiments
414 with no mid-century forcing in 2100 CE because the response time of the simulated glaciers was longer than the
415 40-year period between the present-day and future time slices. The present day and end-of-century mass balances

416　therefore put bounds on glacier evolution, and future work could address this through continuous mass balance
417　modelling in conjunction with ice-flow modelling.
418
419　The uncertainties associated with GCM projections increase with time after 2100 CE, particularly under RCP8.5.
420　For example, forecasts of global climate warming for 2281–2300 CE relative to 1986–2005 CE under RCP8.5
421　range from 3.0°C to 12.6°C (Collins et al., 2013). In the absence of RCMs that can project changes in precipitation
422　after 2100 CE, precipitation was maintained at the same level for the climate-glacier model simulations beyond
423　2100 CE. The end-of-century precipitation amount is unlikely to be reflective of the more distant future and
424　therefore more realistic precipitation projections are required to discover if the active glacier can be sustained
425　further into the future or will lose mass more quickly than expected. However, we expect that there will not be a
426　sufficient increase in precipitation beyond 2100 CE that could compensate for the projected warming under
427　RCP8.5. The projected temperature changes used for the simulations of glacier evolution after 2100 CE are global
428　averages and do not include the effects of elevation-dependent warming. Warming is likely to be higher than the
429　global mean for the Khumbu region given that warming over land is generally at least 0.2°C higher than the global
430　mean value (Collins et al., 2013).
431
4.2 Comparison of outcomes under RCP4.5 and RCP8.5
432
433　Current global greenhouse gas emissions are following the trajectory of the moderate warming scenario RCP4.5,
434　and the extreme warming scenario RCP8.5 could be described as 'low possibility but high impact' (Pedersen et
435　al., 2020). However, mountain regions are warming more rapidly than the global mean such that a global
436　temperature rise of 1.5°C will lead to 2.1 ± 0.1°C of warming in High Mountain Asia (Kraaijenbrink et al., 2017;
437　Pepin et al., 2022) although the occurrence of elevation-dependent warming above 5,000 m a.s.l. is debated (Gao
438　et al., 2018). High-magnitude precipitation events from winter Westerly disturbances increased by up to a factor
439　of seven between the present day and 2100 CE under RCP8.5 and could result in net annual glacier mass balances
440　that are less negative than would be the case when solely forced by change in MAAT. We found no evidence of
441　future increases in precipitation offsetting RCP8.5 warming; net glacier mass balance was strongly negative in all
442　RCP8.5 experiments and insufficient to maintain an actively flowing glacier. Under RCP8.5, glacier mass balance
443　in the monsoon-influenced Himalaya may therefore shift from being driven by accumulation during the monsoon
444　to predominantly during winter, with monsoon precipitation only resulting in snow accumulation at the very
445　highest elevations being insufficient to maintain flowing glaciers. This outcome is avoidable by limiting
446　anthropogenic warming to within RCP4.5, which, due to the associated increase in precipitation, could sustain
447　nearly two thirds of the current glacier volume until 2100 CE and potentially two centuries further into the future.
448
449　Comparing our results to those for the same glacier from a global modelling study forced by an ensemble of 10
450　Global Climate Models (Rounce et al., 2023) shows that our experiments project less severe rates of ice volume
451　decline resulting in a smaller amount of loss by 2100 CE (Fig. 8). In our experiments, there is 39% less loss under
452　RCP4.5 and 32% less under RCP8.5 than in the global study. One difference between these results is that rather
453　than using the global glacier inventory outline to define the glacier margins we consider only the actively flowing
454　glacier and so exclude 20% of the starting glacier volume in the detached tongue. We would expect the two
455　sections of the glacier to evolve along different paths: while the active glacier responds to climate change as
456　projected in our experiments, thick supraglacial debris mantling the detached tongue could allow this ice mass to
457　survive and slowly decay *in situ* for many decades beyond the present day. The decay of the detached tongue may
458　however increase due to erosion of the surface by ice cliffs and supraglacial water bodies that are expanding across
459　the former glacier surface.
460
4.3 Impacts of microscale meteorology on glacier change
461
462　While we have considered the effects of mesoscale meteorology on glacier mass balance, smaller-scale processes
463　operating close to the land surface could also be important. Katabatic winds are suggested to explain a local 15-
464　year decrease in maximum air temperatures and precipitation over glaciers while minimum air temperatures
465　continue to rise (Salerno et al., 2023). However, the impact of micro-scale near-surface cooling on the duration
466　and extent of mesoscale precipitation and accumulation is likely to be minimal, and therefore unlikely to
467　significantly affect glacier-wide mass balance (Mott et al., 2020; Shaw et al., 2024). Observations from an AWS
468　on Khumbu Glacier (6,464 m a.s.l.) indicate that surface energy fluxes may be sufficient to cause non-negligible
469　melting of glacier surfaces despite freezing air temperatures (Matthews et al., 2020). Results from an ice core
470　from South Col Glacier (>8,000 m a.s.l.) combined with COSIPY experiments suggested that ablation may also
471　take place at even at the highest elevations (Potocki et al., 2022). However, a subsequent study of the same glacier
472　found no evidence of change, and identified large uncertainties associated with simulating mass balance at these
473　extreme elevations where sub-daily air temperature gradients and the duration of snow cover strongly affect
474　ablation and accumulation (Brun et al., 2023). Our results show that avalanching and sublimation are important
475　controls on recent and future glacier evolution for Khumbu Glacier. Our study addresses these finer-scale temporal

(hourly) and spatial (100 m) processes that affect glacier mass balance across the elevation range of Khumbu Glacier, but further observations of meteorological and glaciological conditions at the highest elevations would be beneficial (Brun et al., 2023; Khadka et al., 2021; Mölg et al., 2014; Shaw et al., 2022).

4.4 The response of large debris-covered glaciers to climate change

The dynamic response time of large glaciers to climate change is of the order of centuries, and significant changes in glacier volume continue after an imposed forcing ceases. For this reason, we start our simulations from the late Holocene (around 1.3 ka) when Khumbu Glacier was last considered dynamically stable (Hornsey et al., 2022; Rowan et al., 2015). The relationship between response time and mass balance becomes less important after 2100 CE when the glacier is so small that any dynamic behaviour has little impact on volume change. Global and regional glacier modelling studies typically start their simulations in the current century (e.g., 2000–2007 CE (Marzeion et al., 2020); 2015 CE (Rounce et al., 2023) and a further complication arises from the use of global glacier inventories as a starting point for glacier modelling studies, as such inventories cannot capture the current dynamic state of glaciers that are imbalanced, and so include all ice-covered areas rather than identifying actively flowing ice. However, satellite-derived velocity products do identify where ice flow within glacier outlines declines to negligible rates (Dehecq et al., 2019). The RGI 7.0 inventory for Khumbu Glacier is based on imagery from 1999 CE (RGI 7.0 Consortium, 2023) where the detached debris-covered tongue represents 20% of the glacier volume contained within this outline (Fig. 1c). Simulations that integrated the stagnant tongue into the model domain rather than as part of the flowing ice improved the representation of simulated ice flow compared to observed values, supporting our conclusion that the debris-covered tongue has been dynamically detached from the active glacier for 50–100 years (Rowan et al., 2021). Additionally, field observations support the active and stagnant sections co-existing in contact with each other, as englacial optical televiewing indicates that thrusting occurs at several sites denoted by skewed internal debris layers and of basal ice that has been thrust to the glacier surface near to the Changri Nup palaeoconfluence from the direction of Khumbu icefall (Miles et al., 2021). Our simulations show that development of supraglacial debris at the terminus reduces net loss (Fig. 5) but otherwise the glacier surface is clean (Fig. 4). Therefore, while supraglacial debris sustains about 13% of additional glacier volume compared to a clean-ice surface, the local mass balance gradient is a more important control on glacier change for both clean-ice glaciers and debris-covered Himalayan glaciers.

5. Conclusions

In the monsoon-influenced Himalaya, 85% of glacier area is located above 5,000 m and 21% is above 6000 m. Despite these high elevations, Himalayan glaciers are currently rapidly losing ice in response to climate change. Himalayan glaciers are projected to shrink by 53% to 70% during this century due to global climate change. However, the impact of future precipitation change on glacier change remains uncertain because mesoscale meteorology is not represented in current glacier models. We explore the effects of future changes in air temperature and precipitation by simulating the evolution of a benchmark glacier in the monsoon-influenced Nepal Himalaya using mesoscale climate-glacier modelling—Khumbu Glacier in the Everest region of Nepal. The active terminus of Khumbu Glacier is located at 5100 m and the equilibrium line altitude is at 5850 m making Khumbu Glacier representative of many Himalayan glaciers. Historical warming commits Khumbu Glacier to volume loss of 10–23% by 2100 CE. We show that while moderate future warming (RCP4.5) will lead to glacier volume loss of 70% by 2100 CE, the projected concurrent increase in precipitation will offset 34% of this change. However, extreme future warming (RCP8.5) will not be compensated by precipitation but will instead result in substantial ablation above 6,000 m and cause the highest glacier on Earth to vanish by 2160–2260 CE. Our results show that the mass balance of Khumbu Glacier is close to zero by 2100 CE under RCP4.5, although with somewhat different ice volumes remaining depending on the RCM used. Therefore, if climate change is limited to RCP4.5, Khumbu Glacier will lose about a third of its volume and recede to the base of the icefall with insignificant further change. In this scenario, Khumbu Glacier has a similar extent in 2100 CE to the active section of the present-day glacier and is at least one example of how monsoon-influenced Himalayan glaciers could persist into the future if global efforts are sufficient to mitigate anthropogenic climate change.

Code availability

The COSIPY surface energy balance model is publicly available through the repository listed in the online methods. The version of the glacier model iSOSIA used in this study is available from Zenodo: Ann Rowan. (2024). annvrowan/isosia: iSOSIA version used in Schlich-Davies et al. (spm-3.3.3r). Zenodo. https://doi.org/10.5281/zenodo.12666864

Data availability

Daily data from the Coordinated Regional Downscaling Experiment (CORDEX) South Asia domain were downloaded from the Indian Institute of Tropical Meteorology website (http://cccr.tropmet.res.in/home/cordexsa_about.jsp) for the grid box nearest to Khumbu Glacier (27.9065°N, 86.4353°E). Incoming shortwave and longwave radiation components were downloaded from the ESGF portal (https://esgf-ui.ceda.ac.uk/cog/projects/cordex-ceda/).

14 years of meteorological observations were derived from the two Pyramid AWS at 5,050 m a.s.l and at 5,035 m a.s.l (SHARE network Ev-K2-CNR; https://www.evk2cnr.org) and the West Changri Nup glacier AWS at 5,363 m a.s.l (GlacioClim: https://glacioclim.osug.fr/).

Table and caption
557
558 Table 1. Regional Climate Models (RCMs) chosen for use in this study, and details of the Global Circulation
559 Models (GCMs) from which these are derived. The NOAA RCM that was considered most representative of
560 conditions in the Everest region is highlighted in bold.
561

CORDEX South Asia regional climate model	Driving CMIPS global climate model	CMIPS modelling centre	RCM name used in this study	Future precipitation scenario	2100 CE mean temperature change from present day (°C)	
					RCP.4.5	RCP8.5
ITTM-RegCM4	NOAA-GFDL-GFDL-ESM2M	National Oceanic and Atmospheric Administration (NOAA), USA	**NOAA**	**Wet**	**1.4**	**3.8**
IITM-RegCM4	CCCma-CanESM2	Canadian Centre for Climate Modelling and Analysis (CCCma), Canada	CCCma	Moderate	2.2	4.1
IITM-RegCM4	IPSL-CMSA-LR	Institue Pierre-Simon Laplace (IPSL), France	IPSL	Dry	1.6	3.8

562
563
564
565
566
567
568
569

Figures and captions
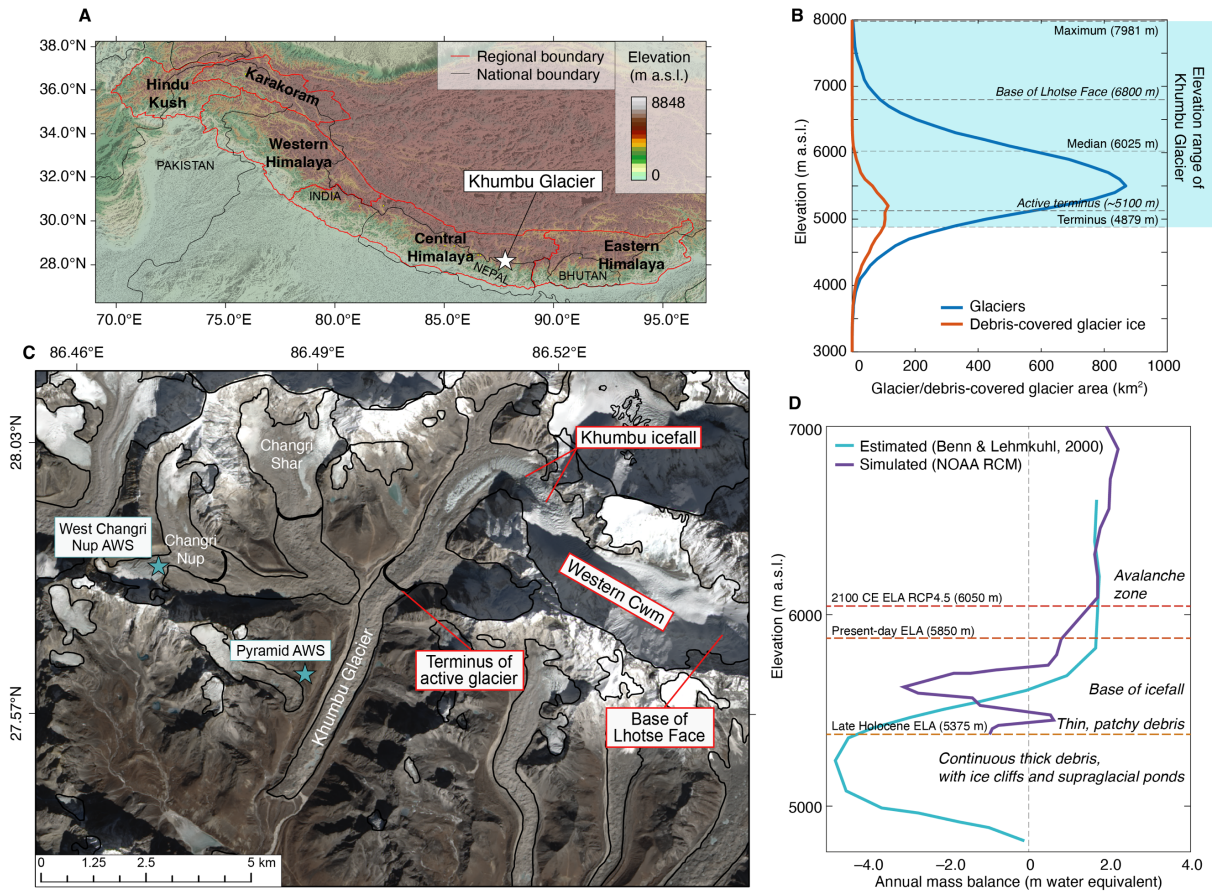
Figure 1: Khumbu Glacier location and context. (a) Location map of High Mountain Asia showing the location of the monsoon-influenced Central and Eastern Himalaya and Khumbu Glacier. (b) hypsometry of glaciers and debris-covered glacier ice in the Central and Eastern Himalaya compared with the elevations of Khumbu Glacier. (c) Satellite image of Khumbu Glacier showing the extent of supraglacial debris, location of the icefall, the extent of active ice flow inferred from observations of glacier velocity (black lines) and location of the automatic weather stations used for RCM downscaling (blue stars). (d) Estimated mass balance gradient for debris-covered glaciers in the Everest region(Benn and Lehmkuhl, 2000) compared with the glacier mass balance gradient simulated using the NOAA RCM and showing change in the equilibrium line altitude (ELA) of Khumbu Glacier in the historical and future simulations for the NOAA RCP4.5 experiment.
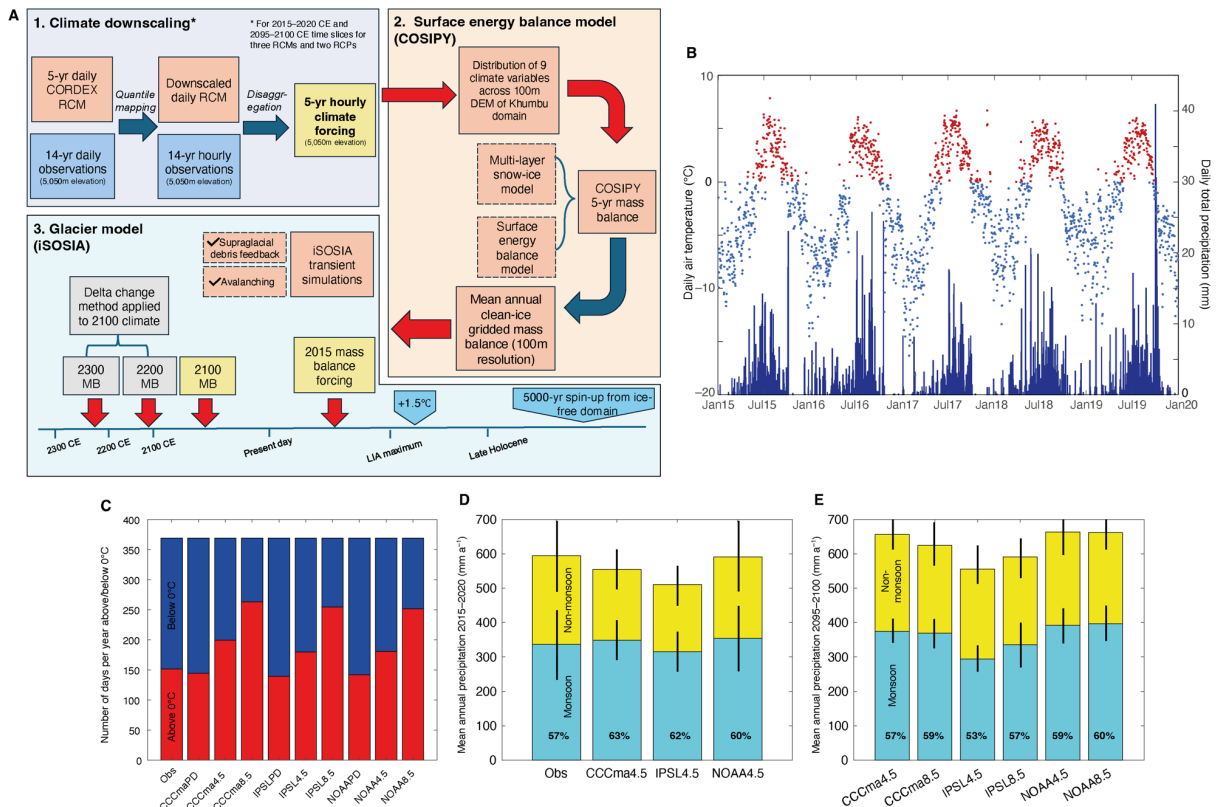
Figure 2: Model experimental design and evaluation of RCM downscaling. (a) Schematic diagram of the climate-glacier modelling approach showing the methods used for downscaling through quantile mapping and disaggregation of climate data. Note that this process does not apply to the post-2100 CE climate forcings which are subject to delta change. Surface energy balance modelling using COSIPY includes the pre-processing stage of meteorological distribution across the Khumbu domain, which is repeated for each RCM in the 2015–2020 CE climates and for the three RCMs and two RCPs for the 2095–2100 CE climates. The simulated mass balance is then used to force the glacier model iSOSIA. (b) Daily mean temperature and daily total precipitation from the NOAA RCM for the present day (2015–2020 CE) following downscaling using quantile mapping with air temperature categorised into above freezing (red) and below freezing (blue). (c) Proportion of air temperatures above and below freezing for the present day for each RCM and RCP for the downscaled daily data compared with observations. (d) Annual precipitation totals for non-monsoon and monsoon with standard deviation between selected years shown by black bars for the downscaled daily data compared with observations. (e) Future (2095–2100 CE) time-slice annual precipitation totals for non-monsoon and monsoon months with standard deviation between selected years shown by black bars. In (d) and (e) the percentage of the total annual precipitation occurring during the monsoon is indicated by the value in bold text. (Obs = meteorological observations from AWS).

13
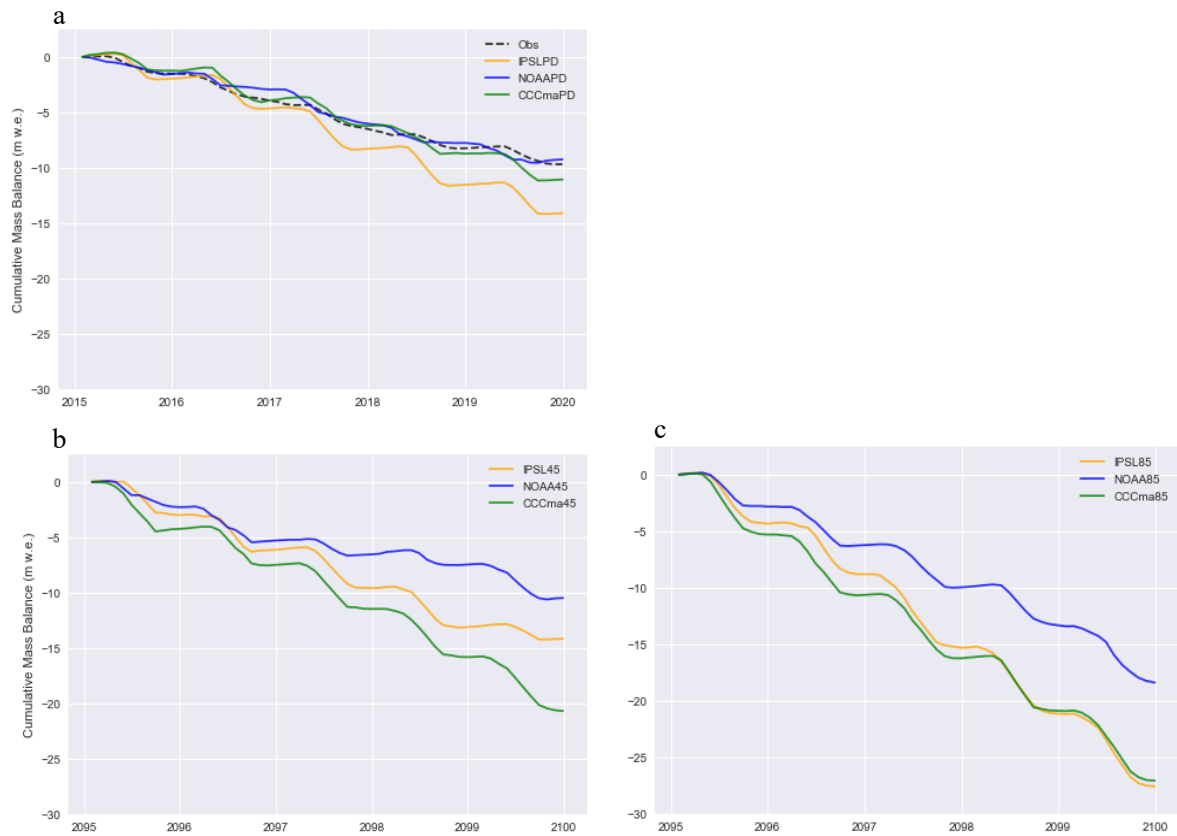
Figure 3: Spatially averaged cumulative clean-ice mass balance with clear seasonality for (a) the present day time-slice including the mass balance forced by the observations used for downscaling, and the end-of-century time-slice under (b) RCP4.5 and (c) RCP8.5. The low annual glacier-wide mass balance values shown here are the result of the extent of the model domain used to force iSOSIA that includes the larger catchment beyond the glacier margins and therefore contains a higher proportion of lower elevations than those of the glacier itself. However the similar mass balance results for simulations forced by NOAA RCM and observations can be clearly seen (a), and the differences between the three RCMs is apparent in all time-slices (a-c).
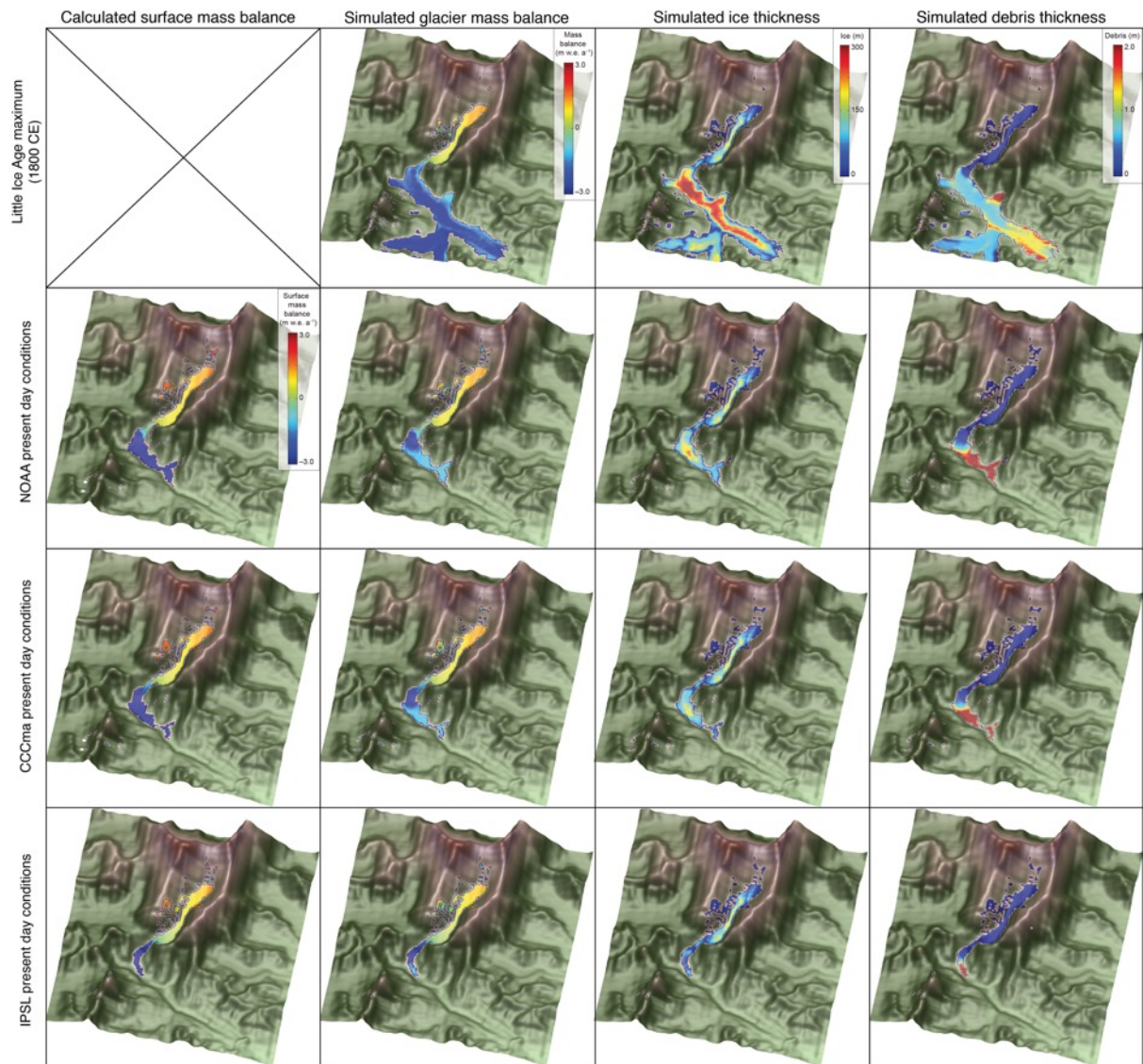
Figure 4. Glacier model sensitivity to surface energy and mass balance forcing, showing Little Ice Age (~1800 CE) glacier mass balance, ice thickness and debris thickness. Present-day results for surface mass balance calculated using each RCM with COSIPY showing glacier mass balance calculated using the same climate forcing following integration with iSOSIA, simulated ice thickness, and simulated debris thickness.
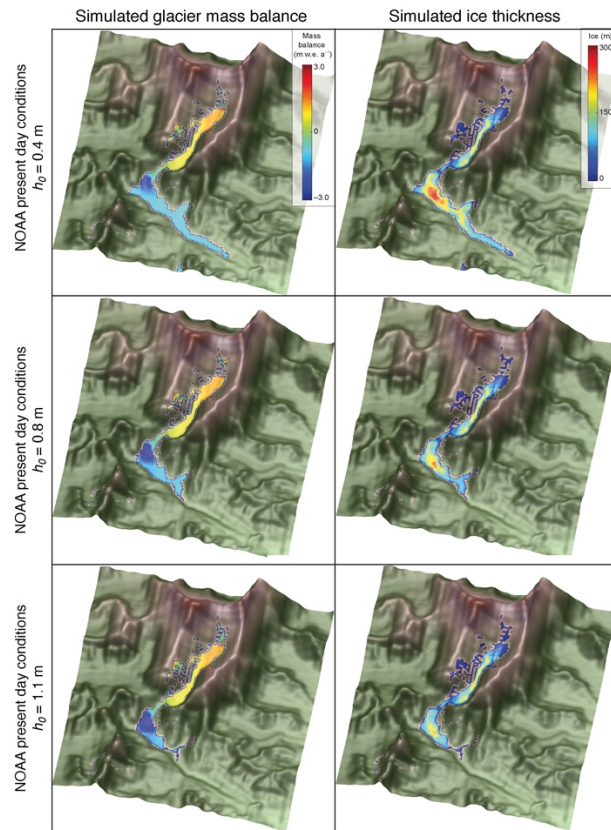
636
637
638   Figure 5. Glacier mass balance and ice thickness simulated using the NOAA climate forcing and the resulting
639   simulated ice thickness for h_0 values of 0.4 m, 0.8 m, and 1.1 m.
640
641
642
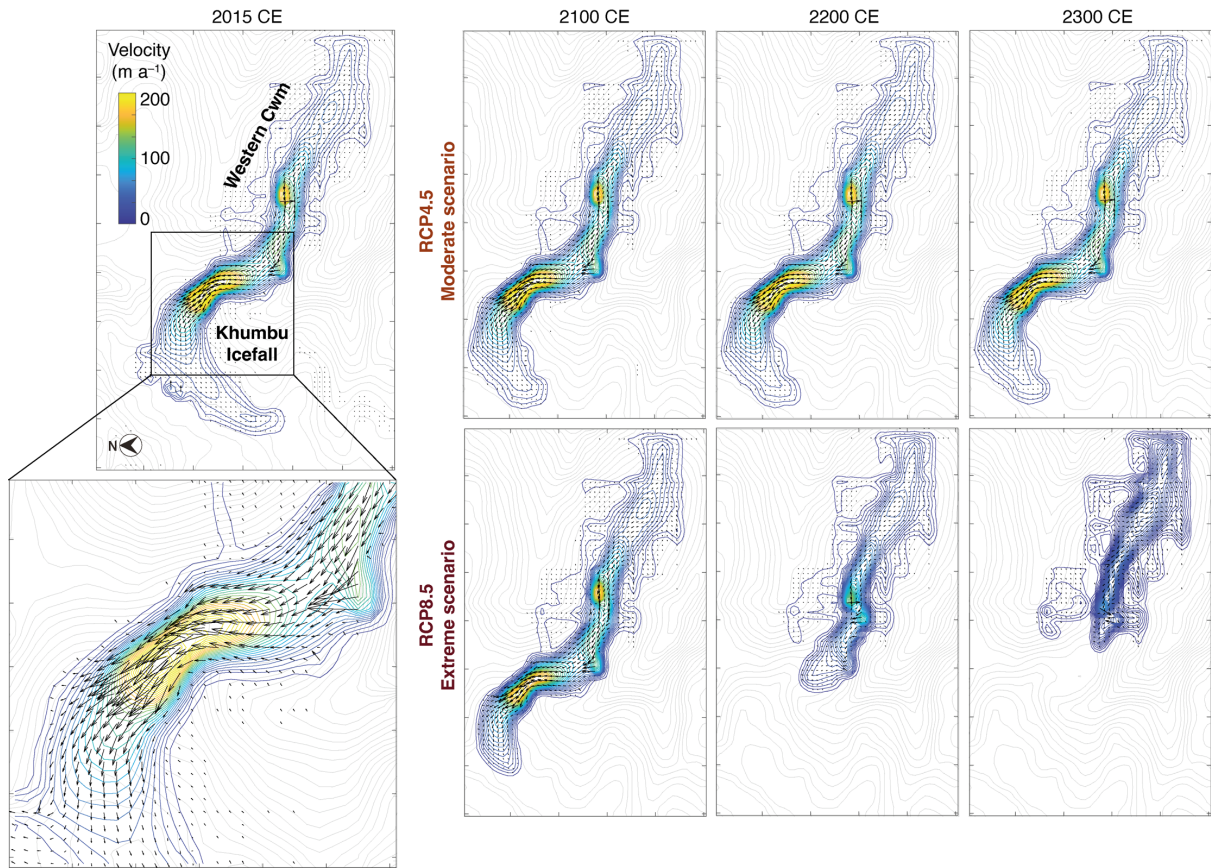
Figure 6. Simulated ice flow for Khumbu Glacier. Velocity-vector maps showing simulated ice flow magnitude and direction from the present day (2015–2020 CE) until 2300 CE under RCP4.5 and RCP8.5 using the downscaled NOAA climate forcing and a value for h_0 of 0.8 m. Simulated ice flow speed is shown as colour shading with blue contours, and the bed topography is shown by grey contours. The outermost contour in each plot represents the slowest ice flow close to the glacier margins with depth-integrated velocities of 5–10 m a^{-1}. Note that rapid flow across the Western Cwm indicated by one arrow shows the effects of avalanching rather than sustained glacier flow.
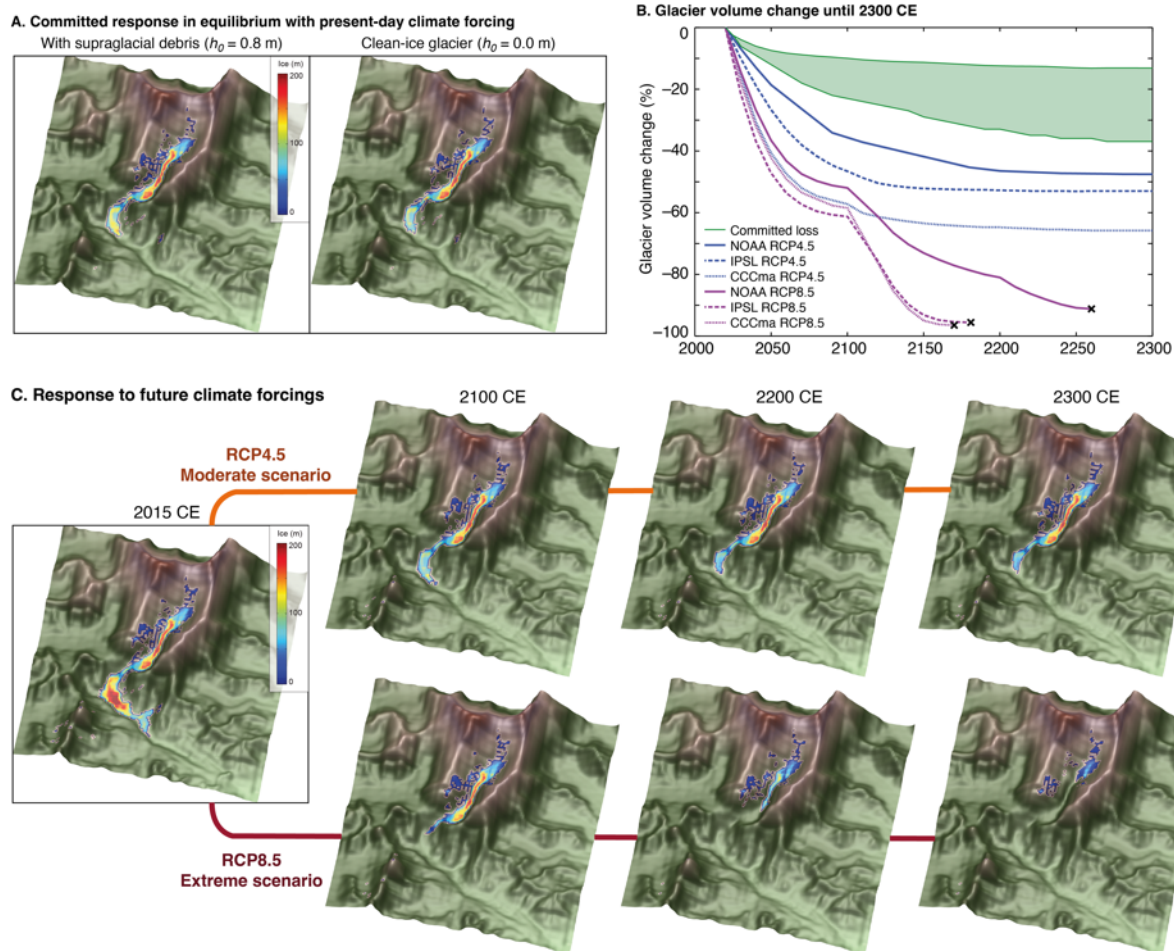
Figure 7. Future glacier volume change projections. (a) Equilibrium ice thickness accounting for the committed response to recent climate change using the downscaled NOAA climate forcing with and without the effect of sub-debris melt. (b) Simulated glacier volume change from the present day (2015–2020 CE) until 2300 CE under RCP4.5 and RCP8.5 for the three downscaled RCMs. The black crosses mark when ice flow has declined sufficiently that the glacier is considered almost absent or no longer viable. The green shading shows the range of the committed volume loss due to historical warming. (c) Simulated ice thickness under RCP4.5 and RCP8.5 for 2100 CE, 2200 CE and 2300 CE using the downscaled NOAA climate forcing.
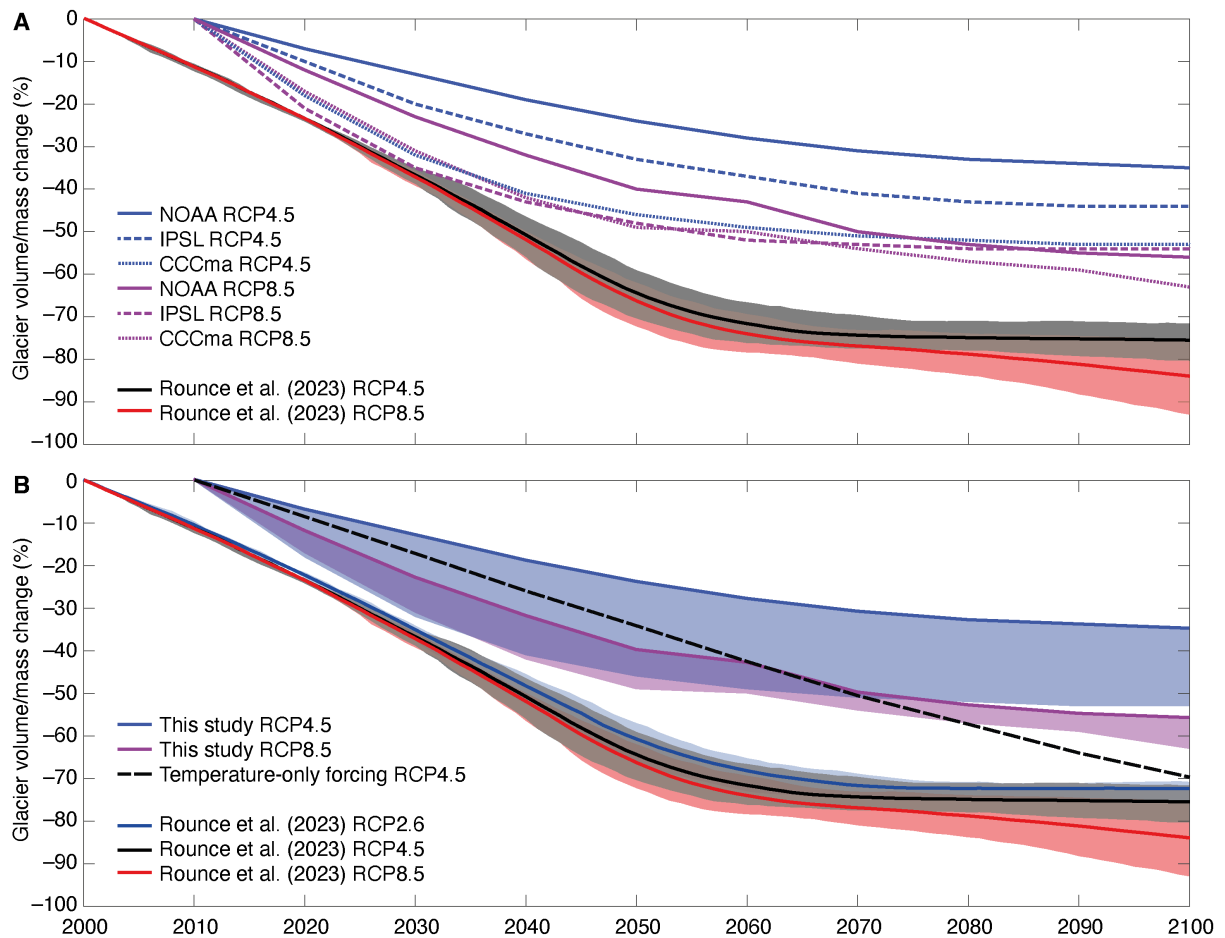
Figure 8. Comparison of projected shrinkage of Khumbu Glacier by 2100 CE from this study with those from Rounce et al. (2023) showing (a) results from each of the six experiments in this study with results from RCP4.5 and RCP8.5 from Rounce et al. (2023), and (b) comparison of results from this study where the bold line shows the NOAA RCP4.5 and RCP8.5 experiments and the black dashed line shows the equivalent result for a simulation where precipitation does not change from the present-day value compared with results from Rounce et al. (2023) for RCP2.6, RCP4.5 and RCP8.5.

References

Altena, B. and Kääb, A.: Ensemble matching of repeat satellite images applied to measure fast-changing ice flow, verified with mountain climber trajectories on Khumbu icefall, Mount Everest, J. Glaciol., 66, 905–915, https://doi.org/10.1017/jog.2020.66, 2020.

Anderson, L. S. and Anderson, R. S.: Modeling debris-covered glaciers: response to steady debris deposition, The Cryosphere, 10, 1105–1124, https://doi.org/10.5194/tc-10-1105-2016, 2016.

Bartlett, O. T., Ng, F. S. L., and Rowan, A. V.: Morphology and evolution of supraglacial hummocks on debris-covered Himalayan glaciers, Earth Surf. Process. Landforms, 46, 525–539, https://doi.org/10.1002/esp.5043, 2021.

Benn, D. I. and Lehmkuhl, F.: Mass balance and equilibrium-line altitudes of glaciers in high-mountain environments, Quaternary International, 65–66, 15–29, https://doi.org/10.1016/S1040-6182(99)00034-8, 2000.

Benn, D. I. and Owen, L. A.: The role of the Indian summer monsoon and the mid-latitude westerlies in Himalayan glaciation: review and speculative discussion, Journal of the Geological Society, 155, 353–363, https://doi.org/10.1144/gsjgs.155.2.0353, 1998.

Bonekamp, P. N. J., Wanders, N., Wiel, K., Lutz, A. F., and Immerzeel, W. W.: Using large ensemble modelling to derive future changes in mountain specific climate indicators in a 2 and 3°C warmer world in High Mountain Asia, Int J Climatol, 41, https://doi.org/10.1002/joc.6742, 2021.

Bookhagen, B. and Burbank, D. W.: Topography, relief, and TRMM-derived rainfall variations along the Himalaya, Geophys. Res. Lett., 33, L08405, https://doi.org/10.1029/2006GL026037, 2006.

Brun, F., King, O., Réveillet, M., Amory, C., Planchot, A., Berthier, E., Dehecq, A., Bolch, T., Fourteau, K., Brondex, J., Dumont, M., Mayer, C., Leinss, S., Hugonnet, R., and Wagnon, P.: Everest South Col Glacier did not thin during the period 1984–2017, The Cryosphere, 17, 3251–3268, https://doi.org/10.5194/tc-17-3251-2023, 2023.

Collins, M., Knutti, R., and Arblaster, J.: Long-term Climate Change: Projections, Commitments and Irreversibility. In: Climate Change 2013: The Physical Science Basis. Contribution of Working Group I to the Fifth Assessment Report of the Intergovernmental Panel on Climate Change [Stocker, T.F., D. Qin, G.-K. Plattner, M. Tignor, S.K. Allen, J. Boschung, A. Nauels, Y. Xia, V. Bex and P.M. Midgley (eds.)]. Cambridge University Press, Cambridge, United Kingdom and New York, NY, USA,, 1–108., 2013.

Debele, B., Srinivasan, R., and Yves Parlange, J.: Accuracy evaluation of weather data generation and disaggregation methods at finer timescales, Advances in Water Resources, 30, 1286–1300, https://doi.org/10.1016/j.advwatres.2006.11.009, 2007.

Dehecq, A., Gourmelen, N., Gardner, A. S., Brun, F., Goldberg, D., Nienow, P. W., Berthier, E., Vincent, C., Wagnon, P., and Trouvé, E.: Twenty-first century glacier slowdown driven by mass loss in High Mountain Asia, Nature Geosci, 12, 22–27, https://doi.org/10.1038/s41561-018-0271-9, 2019.

Egholm, D. L., Knudsen, M. F., Clark, C. D., and Lesemann, J. E.: Modeling the flow of glaciers in steep terrains: The integrated second-order shallow ice approximation (iSOSIA), J. Geophys. Res., 116, https://doi.org/10.1029/2010JF001900, 2011.

Farinotti, D., Huss, M., Fürst, J. J., Landmann, J., Machguth, H., Maussion, F., and Pandit, A.: A consensus estimate for the ice thickness distribution of all glaciers on Earth, Nat. Geosci., 12, 168–173, https://doi.org/10.1038/s41561-019-0300-3, 2019.

Farr, T. G., Rosen, P. A., Caro, E., Crippen, R., Duren, R., Hensley, S., Kobrick, M., Paller, M., Rodriguez, E., Roth, L., Seal, D., Shaffer, S., Shimada, J., Umland, J., Werner, M., Oskin, M., Burbank, D., and Alsdorf, D.: The Shuttle Radar Topography Mission, Reviews of Geophysics, 45, 2005RG000183, https://doi.org/10.1029/2005RG000183, 2007.

Förster, K., Hanzer, F., Winter, B., Marke, T., and Strasser, U.: An open-source MEteoroLOgical observation time series DISaggregation Tool (MELODIST v0.1.1), Geosci. Model Dev., 9, 2315–2333, https://doi.org/10.5194/gmd-9-2315-2016, 2016.

Gades, A., Conway, H., Nereson, N., Naito, N., and Kadota, T.: Radio echo-sounding through supraglacial debris on Lirung and Khumbu Glaciers, Nepal Himalayas, Debris-Covered Glaciers (Proceedings of a workshop held at Seattle, Washington, USA, September 2000). IAHS, 264, 13–22, 2000.

Gao, Y., Chen, F., Lettenmaier, D. P., Xu, J., Xiao, L., and Li, X.: Does elevation-dependent warming hold true above 5000 m elevation? Lessons from the Tibetan Plateau, npj Clim Atmos Sci, 1, 19, https://doi.org/10.1038/s41612-018-0030-z, 2018.

Herreid, S. and Pellicciotti, F.: The state of rock debris covering Earth's glaciers, Nat. Geosci., 13, 621–627, https://doi.org/10.1038/s41561-020-0615-0, 2020.

Hornsey, J., Rowan, A. V., Kirkbride, M. P., Livingstone, S. J., Fabel, D., Rodes, A., Quincey, D. J., Hubbard, B., and Jomelli, V.: Be-10 Dating of Ice-Marginal Moraines in the Khumbu Valley, Nepal, Central Himalaya, Reveals the Response of Monsoon-Influenced Glaciers to Holocene Climate Change, JGR Earth Surface, 127, https://doi.org/10.1029/2022JF006645, 2022.

Huintjes, E., Neckel, N., Hochschild, V., and Schneider, C.: Surface energy and mass balance at Purogangri ice cap, central Tibetan Plateau, 2001–2011, J. Glaciol., 61, 1048–1060, https://doi.org/10.3189/2015JoG15J056, 2015.

Immerzeel, W. W., van Beek, L. P. H., Konz, M., Shrestha, A. B., and Bierkens, M. F. P.: Hydrological response to climate change in a glacierized catchment in the Himalayas, Climatic Change, 110, 721–736, https://doi.org/10.1007/s10584-011-0143-4, 2012.

Kaini, S., Nepal, S., Pradhananga, S., Gardner, T. and Sharma, A. K. 2019. Representative general circulation models selection and downscaling of climate data for the transboundary Koshi river basin in China and Nepal. International Journal of Climatology 40(9): 4131-4149. doi: 10.1002/joc.6447.

Katzenberger, A., Schewe, J., Pongratz, J., and Levermann, A.: Robust increase of Indian monsoon rainfall and its variability under future warming in CMIP6 models, Earth Syst. Dynam., 12, 367–386, https://doi.org/10.5194/esd-12-367-2021, 2021.

Khadka, A., Matthews, T., Perry, L. B., Koch, I., Wagnon, P., Shrestha, D., Sherpa, T. C., Aryal, D., Tait, A., Sherpa, T. G., Tuladhar, S., Baidya, S. K., Elvin, S., Elmore, A. C., Gajurel, A., and Mayewski, P. A.: Weather on MOUNT EVEREST during the 2019 summer MONSOON, Weather, 76, 205–207, https://doi.org/10.1002/wea.3931, 2021.

King, O., Bhattacharya, A., Ghuffar, S., Tait, A., Guilford, S., Elmore, A. C., and Bolch, T.: Six Decades of Glacier Mass Changes around Mt. Everest Are Revealed by Historical and Contemporary Images, One Earth, 3, 608–620, https://doi.org/10.1016/j.oneear.2020.10.019, 2020.

Kraaijenbrink, P. D. A., Bierkens, M. F. P., Lutz, A. F., and Immerzeel, W. W.: Impact of a global temperature rise of 1.5 degrees Celsius on Asia's glaciers, Nature, 549, 257–260, https://doi.org/10.1038/nature23878, 2017.

Lafon, T. et al. 2012. Bias correction of daily precipitation simulated by a regional climate model: A comparison of methods, International Journal of Climatology 33(6): 1367–1381. doi:10.1002/joc.3518.

Luo, M. et al. (2018). Comparing bias correction methods used in downscaling precipitation and temperature from regional climate models: A case study from the Kaidu River basin in western China. Water 10(8): 1046. doi:10.3390/w10081046.

Lutz, A., Maat, H., Biemans, H., Shrestha, A., Wester, P. and Immerzeel, W., (2016). Selecting representative climate models for climate change impact studies: an advanced envelope-based selection approach. International Journal of Climatology 36(12): 3988-4005.

Maraun D, Wetterhall F, Ireson AM, Chandler RE. Kendon EJ, Widmann M. Brienen S. Rust H. W. Sauter T. Themeßl M. Venema V. K. C. 2010 Precipitation downscaling under climate change: recent developments to bridge the gap between dynamical models and the end user. Reviews of Geophysics 48 (3), RG3003.

Marzeion, B., Hock, R., Anderson, B., Bliss, A., Champollion, N., Fujita, K., Huss, M., Immerzeel, W. W., Kraaijenbrink, P., Malles, J., Maussion, F., Radić, V., Rounce, D. R., Sakai, A., Shannon, S., Van De Wal, R., and Zekollari, H.: Partitioning the Uncertainty of Ensemble Projections of Global Glacier Mass Change, Earth's Future, 8, e2019EF001470, https://doi.org/10.1029/2019EF001470, 2020.

Matthews, T., Perry, L. B., Koch, I., Aryal, D., Khadka, A., Shrestha, D., Abernathy, K., Elmore, A. C., Seimon, A., Tait, A., Elvin, S., Tuladhar, S., Baidya, S. K., Potocki, M., Birkel, S. D., Kang, S., Sherpa, T. C., Gajurel, A., and Mayewski, P. A.: Going to Extremes: Installing the World's Highest Weather Stations on Mount Everest, Bulletin of the American Meteorological Society, 101, E1870–E1890, https://doi.org/10.1175/BAMS-D-19-0198.1, 2020.

Maurer, J. M., Schaefer, J. M., Rupper, S., and Corley, A.: Acceleration of ice loss across the Himalayas over the past 40 years, Sci. Adv., 5, eaav7266, https://doi.org/10.1126/sciadv.aav7266, 2019.

Miles, E. S., Willis, I., Buri, P., Steiner, J. F., Arnold, N. S., and Pellicciotti, F.: Surface Pond Energy Absorption Across Four Himalayan Glaciers Accounts for 1/8 of Total Catchment Ice Loss, Geophys. Res. Lett., 45, https://doi.org/10.1029/2018GL079678, 2018a.

Miles, K. E., Hubbard, B., Quincey, D. J., Miles, E. S., Sherpa, T. C., Rowan, A. V., and Doyle, S. H.: Polythermal structure of a Himalayan debris-covered glacier revealed by borehole thermometry, Sci Rep, 8, 16825, https://doi.org/10.1038/s41598-018-34327-5, 2018b.

Miles, K. E., Hubbard, B., Miles, E. S., Quincey, D. J., Rowan, A. V., Kirkbride, M., and Hornsey, J.: Continuous borehole optical televiewing reveals variable englacial debris concentrations at Khumbu Glacier, Nepal, Commun Earth Environ, 2, 12, https://doi.org/10.1038/s43247-020-00070-x, 2021.

Mölg, T., Maussion, F., and Scherer, D.: Mid-latitude westerlies as a driver of glacier variability in monsoonal High Asia, Nature Clim Change, 4, 68–73, https://doi.org/10.1038/nclimate2055, 2014.

Mott, R., Stiperski, I., and Nicholson, L.: Spatio-temporal flow variations driving heat exchange processes at a mountain glacier, The Cryosphere, 14, 4699–4718, https://doi.org/10.5194/tc-14-4699-2020, 2020.

Nakawo, M., Iwata, S., Watanabe, O. and Yoshida, M.: Processes which distribute supraglacial debris on the Khumbu Glacier, Nepal Himalaya. Annals of Glaciology, 8, pp.129-131, https://doi.org/10.3189/S0260305500001294, 1986.

Nicholson, L., Wirbel, A., Mayer, C., and Lambrecht, A.: The Challenge of Non-Stationary Feedbacks in Modeling the Response of Debris-Covered Glaciers to Climate Forcing, Front. Earth Sci., 9, 662695, https://doi.org/10.3389/feart.2021.662695, 2021.

Owen, L. A., Robinson, R., Benn, D. I., Finkel, R. C., Davis, N. K., Yi, C., Putkonen, J., Li, D., and Murray, A. S.: Quaternary glaciation of Mount Everest, Quaternary Science Reviews, 28, 1412–1433, https://doi.org/10.1016/j.quascirev.2009.02.010, 2009.

Pedersen, J. S. T., Van Vuuren, D. P., Aparício, B. A., Swart, R., Gupta, J., and Santos, F. D.: Variability in historical emissions trends suggests a need for a wide range of global scenarios and regional analyses, Commun Earth Environ, 1, 41, https://doi.org/10.1038/s43247-020-00045-y, 2020.

Pellicciotti, F., Stephan, C., Miles, E., Herreid, S., Immerzeel, W. W., and Bolch, T.: Mass-balance changes of the debris-covered glaciers in the Langtang Himal, Nepal, from 1974 to 1999, J. Glaciol., 61, 373–386, https://doi.org/10.3189/2015JoG13J237, 2015.

Pepin, N. C., Arnone, E., Gobiet, A., Haslinger, K., Kotlarski, S., Notarnicola, C., Palazzi, E., Seibert, P., Serafin, S., Schöner, W., Terzago, S., Thornton, J. M., Vuille, M., and Adler, C.: Climate Changes and Their Elevational Patterns in the Mountains of the World, Reviews of Geophysics, 60, https://doi.org/10.1029/2020RG000730, 2022.

Piani, C. et al. 2010. Statistical Bias Correction of global simulated daily precipitation and temperature for the application of Hydrological Models. Journal of Hydrology 395(3–4): 199–215. doi:10.1016/j.jhydrol.2010.10.024.

Pierce, D. W., Barnett, T. P., Santer, B. D., and Gleckler, P. J.: Selecting global climate models for regional climate change studies, Proc. Natl. Acad. Sci. U.S.A., 106, 8441–8446, https://doi.org/10.1073/pnas.0900094106, 2009.

Potocki, M., Mayewski, P. A., Matthews, T., Perry, L. B., Schwikowski, M., Tait, A. M., Korotkikh, E., Clifford, H., Kang, S., Sherpa, T. C., Singh, P. K., Koch, I., and Birkel, S.: Mt. Everest's highest glacier is a sentinel for accelerating ice loss, npj Clim Atmos Sci, 5, 7, https://doi.org/10.1038/s41612-022-00230-0, 2022.

Pritchard, H. D.: Asia's shrinking glaciers protect large populations from drought stress, Nature, 569, 649–654, https://doi.org/10.1038/s41586-019-1240-1, 2019.

Quincey, D. J., Luckman, A., and Benn, D.: Quantification of Everest region glacier velocities between 1992 and 2002, using satellite radar interferometry and feature tracking, J. Glaciol., 55, 596–606, https://doi.org/10.3189/002214309789470987, 2009.

Ragettli, S., Immerzeel, W. W., and Pellicciotti, F.: Contrasting climate change impact on river flows from high-altitude catchments in the Himalayan and Andes Mountains, Proc Natl Acad Sci USA, 113, 9222–9227, https://doi.org/10.1073/pnas.1606526113, 2016.

Reiter, P., Gutjahr, O., Schefczyk, L., Heinemann, G. and Casper, M. 2017. Does applying quantile mapping to subsamples improve the bias correction of daily precipitation? International Journal of Climatology 38(4): 1623–1633. doi:10.1002/joc.5283.

RGI 7.0 Consortium: A Dataset of Global Glacier Outlines, Version 7.0. Boulder, Colorado USA. NSIDC: National Snow and Ice Data Center, https://doi.org/10.5067/f6jmovy5navz, 2023.

Roering, J. J., Kirchner, J. W., and Dietrich, W. E.: Evidence for nonlinear, diffusive sediment transport on hillslopes and implications for landscape morphology, Water Resources Research, 35, 853–870, https://doi.org/10.1029/1998WR900090, 1999.

Rounce, D. R., Hock, R., Maussion, F., Hugonnet, R., Kochtitzky, W., Huss, M., Berthier, E., Brinkerhoff, D., Compagno, L., Copland, L., Farinotti, D., Menounos, B., and McNabb, R. W.: Global glacier change in the 21st century: Every increase in temperature matters, Science, 379, 78–83, https://doi.org/10.1126/science.abo1324, 2023.

Rowan, A. V., Egholm, D. L., Quincey, D. J., and Glasser, N. F.: Modelling the feedbacks between mass balance, ice flow and debris transport to predict the response to climate change of debris-covered glaciers in the Himalaya, Earth and Planetary Science Letters, 430, 427–438, https://doi.org/10.1016/j.epsl.2015.09.004, 2015.

Rowan, A. V., Egholm, D. L., Quincey, D. J., Hubbard, B., King, O., Miles, E. S., Miles, K. E., and Hornsey, J.: The Role of Differential Ablation and Dynamic Detachment in Driving Accelerating Mass Loss From a Debris-Covered Himalayan Glacier, J. Geophys. Res. Earth Surf., 126, https://doi.org/10.1029/2020JF005761, 2021.

Salerno, F., Guyennon, N., Yang, K., Shaw, T. E., Lin, C., Colombo, N., Romano, E., Gruber, S., Bolch, T., Alessandri, A., Cristofanelli, P., Putero, D., Diolaiuti, G., Tartari, G., Verza, G., Thakuri, S., Balsamo, G.,

870   Miles, E. S., and Pellicciotti, F.: Local cooling and drying induced by Himalayan glaciers under global
871   warming, Nat. Geosci., 16, 1120–1127, https://doi.org/10.1038/s41561-023-01331-y, 2023.
872 Sanjay, J., Krishnan, R., Shrestha, A. B., Rajbhandari, R., and Ren, G.-Y.: Downscaled climate change
873   projections for the Hindu Kush Himalayan region using CORDEX South Asia regional climate models,
874   Advances in Climate Change Research, 8, 185–198, https://doi.org/10.1016/j.accre.2017.08.003, 2017.
875 Sauter, T., Arndt, A., and Schneider, C.: COSIPY v1.3 – an open-source coupled snowpack and ice surface
876   energy and mass balance model, Geosci. Model Dev., 13, 5645–5662, https://doi.org/10.5194/gmd-13-
877   5645-2020, 2020.
878 Shaw, T. E., Miles, E. S., Chen, D., Jouberton, A., Kneib, M., Fugger, S., Ou, T., Lai, H.-W., Fujita, K., Yang,
879   W., Fatichi, S., and Pellicciotti, F.: Multi-decadal monsoon characteristics and glacier response in High
880   Mountain Asia, Environ. Res. Lett., 17, 104001, https://doi.org/10.1088/1748-9326/ac9008, 2022.
881 Shaw, T. E., Buri, P., McCarthy, M., Miles, E. S., and Pellicciotti, F.: Local Controls on Near-Surface Glacier
882   Cooling Under Warm Atmospheric Conditions, JGR Atmospheres, 129, e2023JD040214,
883   https://doi.org/10.1029/2023JD040214, 2024.
884 Shea, J. M., Immerzeel, W. W., Wagnon, P., Vincent, C., and Bajracharya, S.: Modelling glacier change in the
885   Everest region, Nepal Himalaya, The Cryosphere, 9, 1105–1128, https://doi.org/10.5194/tc-9-1105-2015,
886   2015.
887 Sherpa SF, Wagnon P, Brun F, Berthier E, Vincent C, Lejeune Y, Arnaud Y, Kayastha RB, Sinisalo A. 2017.
888   Contrasted surface mass balances of debris-free glaciers observed between the southern and the inner
889   parts of the Everest region (2007–15). Journal of Glaciology 63:637–651. DOI: 10.1017/jog.2017.30
890 Strickland, R. M., Covington, M. D., Gulley, J. D., Kayastha, R. B., and Blackstock, J. M.: Englacial Drainage
891   Drives Positive Feedback Depression Growth on the Debris-Covered Ngozumpa Glacier, Nepal,
892   Geophysical Research Letters, 50, e2023GL104389, https://doi.org/10.1029/2023GL104389, 2023.
893 Watson, C. S., Quincey, D. J., Smith, M. W., Carrivick, J. L., Rowan, A. V., and James, M. R.: Quantifying ice
894   cliff evolution with multi-temporal point clouds on the debris-covered Khumbu Glacier, Nepal, J.
895   Glaciol., 63, 823–837, https://doi.org/10.1017/jog.2017.47, 2017.
896 Wagnon, P., Lafaysse, M., Lejeune, Y., Maisincho, L., Rojas, M. and Chazarin, J.P., 2009. Understanding and
897   modeling the physical processes that govern the melting of snow cover in a tropical mountain
898   environment in Ecuador. Journal of Geophysical Research: Atmospheres 114(D19).
899
900
901